JOURNAL OF MATERIALS SCIENCE **37** (2002) 3149–3154

Powder effects in SiC matrix layered structures fabricated using selective area laser deposition vapor infiltration (SALDVI)

J. E. CROCKER, L. L. SHAW, H. L. MARCUS
Institute of Materials Science, Department of Metallurgy and Materials Engineering, University of Connecticut, Storrs, CT 06268
E-mail: hmarcus@mail.ims.uconn.edu

Silicon carbide has been deposited by laser-induced chemical vapor infiltration from the gas precursor tetramethylsilane, $Si(CH_3)_4$, into loosely packed powder layers of SiC, ZrO_2-Y_2O_3, or Mo. The goal is to produce dense layered structures of arbitrary shape by computer controlled laser scanning where the pore spaces between the powder particles are filled with solid material deposited from the gas phase using the selective area laser deposition vapor infiltration (SALDVI) process. Layered samples were fabricated for each powder material using both single line (bar) and multiple line (slab) laser scan patterns and 10 Torr $Si(CH_3)_4$, 2.5 μm/s scan speed, 1000°C target temperature, and 120 μm layer thickness. Samples of SiC and ZrO_2-Y_2O_3 are prone to surface cracking in the bar geometry, and cracking and delamination of layers in the slab geometry. Samples fabricated with Mo powder have no cracks or delamination defects in either bar or slab geometry as well as a better surface appearance.

1. Introduction

Solid freeform fabrication (SFF) is a manufacturing technique that produces three dimensional shapes from computer representations using additive formation steps. SALDVI is a layer-by-layer approach to SFF in which porous layers of loose powders are densified by depositing solid material from gas precursors into the pore spaces using laser chemical vapor infiltration (CVI) [1]. Because the CVI process can deposit a variety of desirable materials in pure form, SALDVI is capable of building ceramic and composite net shapes and shapes with functionally graded compositions such as embedded devices [2] in a single machine. SALDVI using the SiC-forming gas $Si(CH_3)_4$ with both ceramic [3] and metal [4] powders has been previously investigated. The laser induced temperature distribution, gas precursor pressure, laser scanning speed, and the particle size and properties of the starting powder were found to affect the shape and densification rate of the infiltrated region as well as the final mechanical properties. The appropriate experimental processing parameters were identified to yield greater than 90% dense material in the desired process zone while minimizing extraneous vapor deposition outside to the process zone. The nanocrystalline nature of the solid material deposited from the $Si(CH_3)_4$ gas precursor by laser CVD on solid ceramic substrates has also been well characterized on the micro and atomic scales using XRD, TEM, Raman, and NMR [5]. In this work we investigate the role that the properties of the starting powder plays in the formation of defects during SALDVI processing.

2. Experiment

The SALDVI workstation consists of a vacuum chamber, a powder delivery system, a 50 watt continuous wave CO_2 (10.6 μm wavelength) laser, an xy table with scanning mirrors, and an optical pyrometer temperature probe with a 2 mm diameter sampling size. The laser beam spot size was nominally 1 mm in diameter at the focal point and Gaussian in shape. All components are computer controlled. During SALDVI processing, the surface temperature of the workpiece in the laser-heated process zone is continually monitored by the optical pyrometer. This temperature signal is used in a feedback loop to adjust the laser output power as necessary to achieve a desired processing temperature selected by the operator, termed the target temperature, throughout the experiment. Considering that the laser beam has a Gaussian intensity distribution and a smaller spot size than the pyrometer, the surface temperature within the pyrometer sampling area is non-uniform. Thus the target temperature represents an average temperature in the process zone. The experimental conditions used here in depositing the SiC matrix include 10 Torr $Si(CH_3)_4$ gas pressure, 2.5 μm/s laser scanning speed, and 1000°C target temperature. Three types of powders are investigated in this work, Mo, SiC, and ZrO_2 stabilized with 10–15 weight percent Y_2O_3. Powder size for each is -325 mesh, with particle diameters ranging from a few μm up to 44 μm. The SiC and ZrO_2-Y_2O_3 powders are irregular in shape, while the Mo is spherical. Due to their differing shapes and theoretical densities, the initial packing fraction of the Mo powder bed is higher than the other two, with a

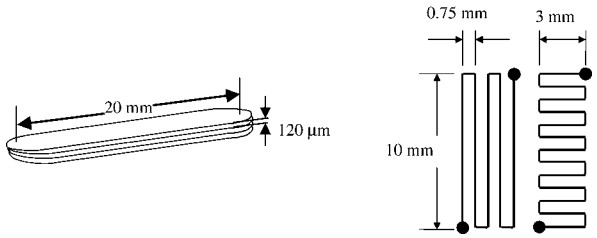

Figure 1 (a) Bar geometry and (b) scan patterns on alternating layers for slab geometry.

solid fraction of 0.55 compared to 0.44. Two laser scan patterns were used to yield either a bar or a slab. The bar geometry consisted of a single pass 20 mm long and three layers high at 120 μm per layer (Fig. 1a). The slab geometry consisted of a rectangle 10 mm long by 3 mm wide and was produced using a line spacing of 0.75 mm and 120 μm layers. Two scan patterns with orthogonal scan directions were used on alternating layers as shown in Fig. 1b. After SALDVI processing, the samples were sectioned and the structure examined in an optical microscope.

3. Results

3.1. Bar geometry/3 layers

The top surfaces of the bars of ZrO_2-Y_2O_3, SiC, and Mo powders after vapor infiltration with SiC are compared in Fig. 2. It is apparent that the width of the bar varies with the type of starting powder, increasing from ZrO_2-Y_2O_3 to SiC to Mo. The surface appearance is also powder dependent, with the smoothest surface obtained using the Mo powder.

Each bar was sectioned parallel to the path of the laser beam as indicated by the arrows in Fig. 2. Representative cross-sections are shown in Figs 3–5 for SiC, ZrO_2-Y_2O_3, and Mo powders respectively. The third layer is located at the top of each figure. The different phases consist of the vapor deposited matrix, the powder particles, and dark regions of unfilled porosity. Details of the top two layers are shown in Figs 3b–5b. For each bar there is continuous material between layers with no gaps or delaminations. Each individual layer consists of two distinct regions. There is a region of vapor infiltrated powder about 70–80 μm thick adjacent to a 40–50 μm thick region of pure vapor deposited material. The SiC powder/SiC matrix bar has surface cracks extending about 100–200 μm into the bar from the surface (Fig. 3). The ZrO_2-Y_2O_3 powder/SiC matrix bar has cracks that extend through all three layers (Fig. 4a) as well as shorter surface cracks (Fig. 4b). The Mo powder/SiC matrix bar has no cracks (Fig. 5).

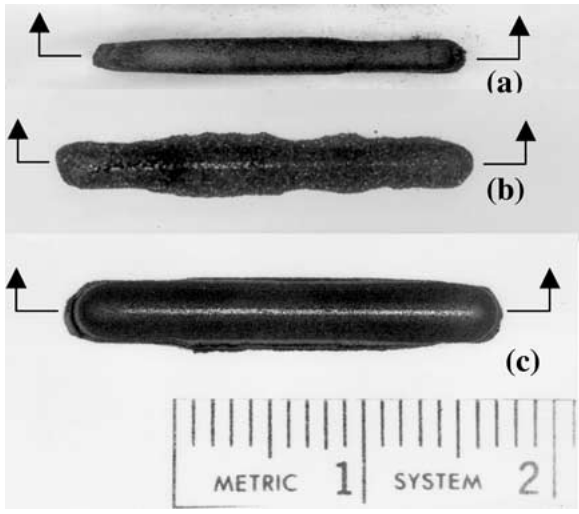

Figure 2 As fabricated ZrO_2-Y_2O_3 (a), SiC (b), and Mo (c) powder/SiC matrix bars.

3.2. Slab/4–6 layers

The 10 mm by 3 mm slab samples were sectioned along the long axis at about mid-width. Figs 6–8 show the as fabricated slabs before sectioning and a representative cross-section through the thickness for the SiC powder/SiC matrix, ZrO_2-Y_2O_3 powder/SiC matrix, and Mo powder/SiC matrix samples respectively. The SiC powder and ZrO_2-Y_2O_3 powder slabs consisted of 4 layers, while the Mo powder slab had 6 layers. The Mo sample has the smoothest surface appearance, while the SiC and ZrO_2-Y_2O_3 samples are rougher and less uniform. The layers consist of infiltrated powder adjacent to regions of pure vapor deposited material, similar to the bar geometry samples. The SiC powder/SiC matrix slab cross-section (Fig. 6b) shows numerous defects, including delaminations between layers, gaps between adjacent lines within a given layer, and surface cracks. The ZrO_2-Y_2O_3 powder/SiC matrix slab cross-section (Fig. 7b) also shows these defect features. The Mo powder/SiC matrix slab cross-section (Fig. 8b) shows neither delaminations nor cracks.

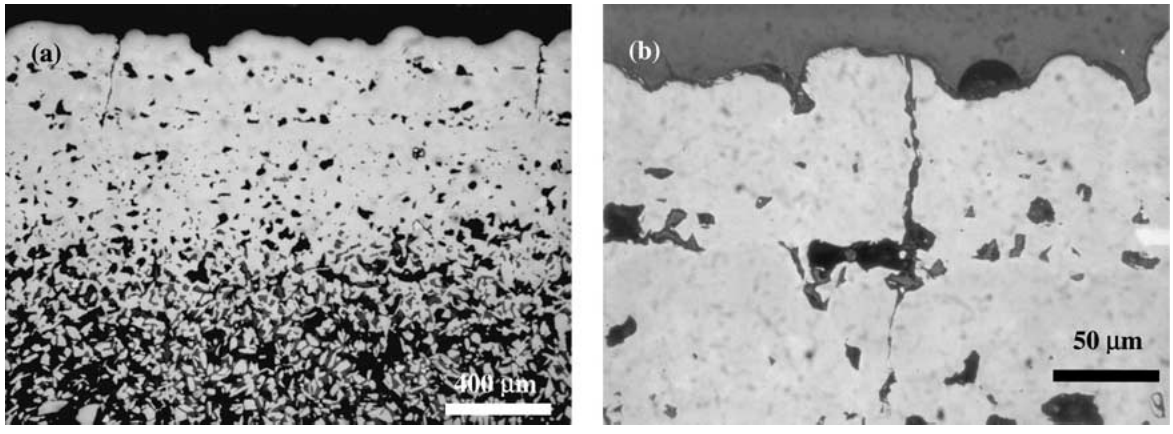

Figure 3 3 layer SiC powder/SiC matrix bar (a) and surface crack through the first layer (b).

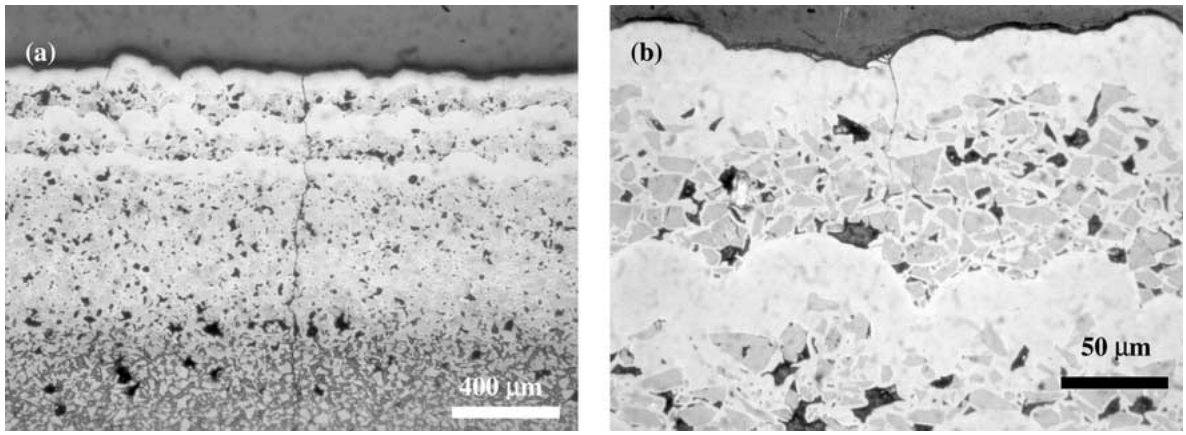

Figure 4 3 layer ZrO_2-Y_2O_3 powder/SiC matrix bar (a) and surface crack (b).

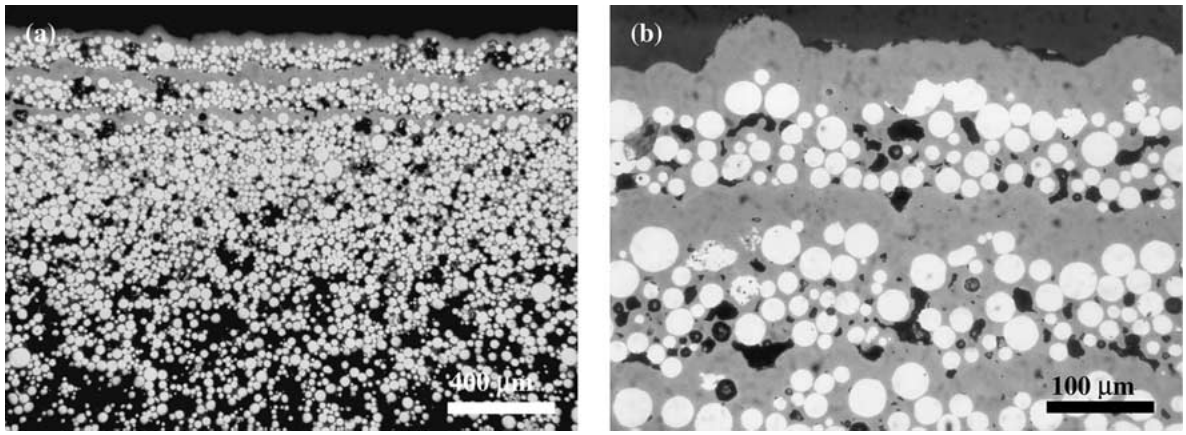

Figure 5 3 layer Mo powder/SiC matrix bar (a) and surface layer with no cracks (b).

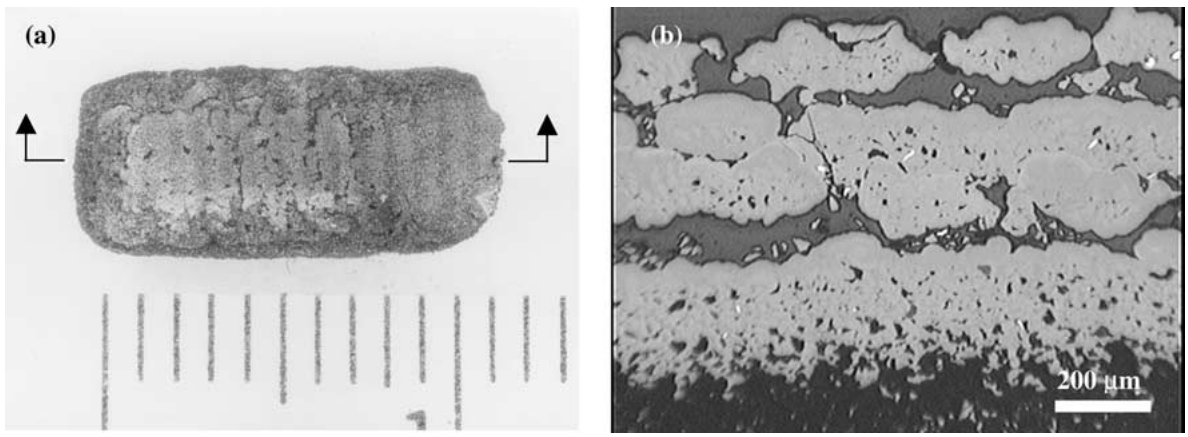

Figure 6 SiC powder/SiC matrix slab with 4 layers (a) as-fabricated and (b) cross-section across layers.

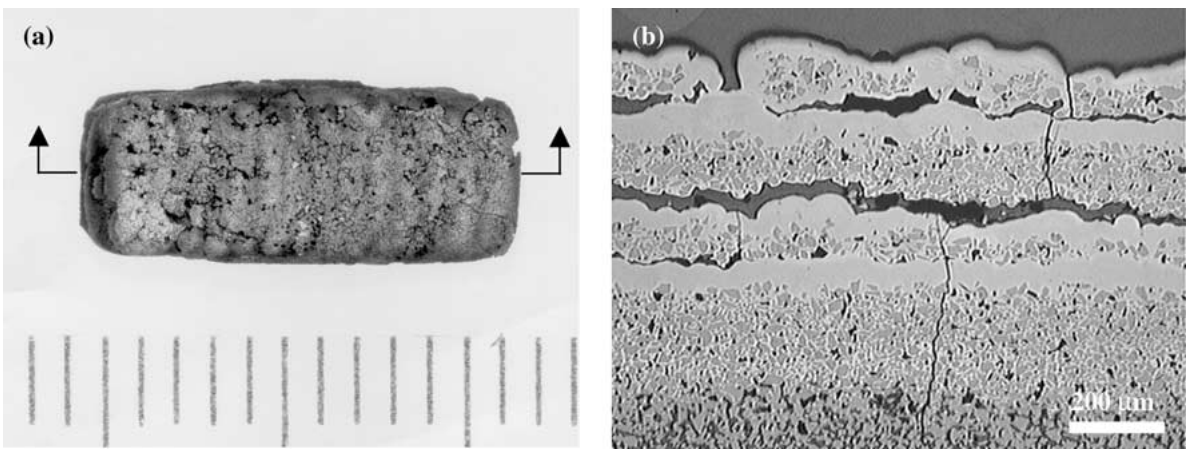

Figure 7 ZrO_2-Y_2O_3 powder/SiC matrix slab with 4 layers (a) as-fabricated and (b) cross-section across layers.

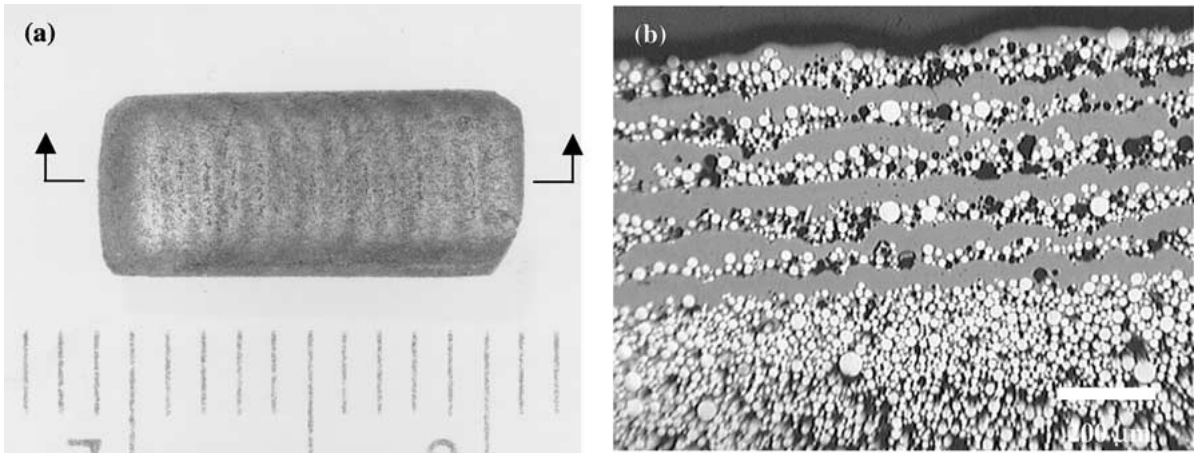

Figure 8 Mo powder/SiC matrix slab with 6 layers (a) as-fabricated and (b) cross-section across layers.

4. Discussion

Different types of defects arise during the densification of SiC and ZrO_2-Y_2O_3 powder layers by laser chemical vapor infiltration of SiC using the SALDVI process. These defects do not appear when Mo powder is used. In the bar geometry, consisting of a single line in each layer, the SiC powder sample has short surface cracks. The ZrO_2-Y_2O_3 powder sample has short surface cracks and long cracks that span the entire sample thickness. There were no delaminations between adjacent layers in the bar geometry. In the slab geometry, consisting of multiple lines within each layer spaced 0.75 mm apart, the SiC and ZrO_2-Y_2O_3 powder samples have delaminations between adjacent layers in addition to surface cracks.

In both the bar and slab geometry, alternating regions of infiltrated powder and pure vapor deposited material are observed through the sample thickness. During the infiltration of each 120 μm thick layer, vapor deposition occurs faster at the surface and slower in the interior. This is due to the higher temperature and more rapid mass transport of gas reactants and products at the surface. It is possible to obtain continuous solid material across layers, as in Fig. 8b for the Mo powder/SiC matrix slab, but the distribution is non-uniform.

The thermal expansion behavior of the three materials (SiC, ZrO_2, and Mo) is shown in Fig. 9 over the range of processing temperatures encountered during SALDVI [6]. A significant thermal expansion mismatch would result in large tensile stresses across the particle/matrix interface after cooling to room temperature from the SALDVI processing temperature. There is a small expansion mismatch between the SiC matrix and the ZrO_2 and Mo powders. No mismatch is expected between the SiC matrix and the SiC powder. Failure of the particle/matrix interface does not appear to occur in the samples with ZrO_2-Y_2O_3 and Mo powder (Figs 4b and 5b), so thermal expansion effects are likely to be small. Thus it is unlikely that thermal expansion mismatch causes for the types of defects observed here.

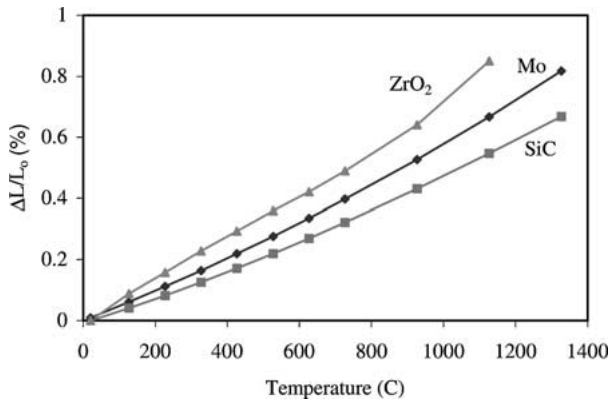

Figure 9 Percent linear thermal expansion for SALDVI materials [6].

One of the significant differences between these three powder materials is their thermal conductivity. Values of the temperature dependent thermal conductivity for Mo, ZrO_2, and two types of SiC are compared in Fig. 10 [7]. It is well known that the thermal conductivity of a material depends on its crystallinity, grain size, and purity. Due to the nanocrystalline nature of the vapor deposited SiC matrix [5], we would expect its thermal conductivity to be less than that of the highly crystalline SiC powder. Thus, the thermal conductivity of the SiC matrix is approximated by the lower curve and that of the SiC powder by the upper curve in Fig. 10. SALDVI structures consist of non-interacting particles in a continuous matrix, so we are concerned with heat flow in a two-phase system, neglecting the approximately 5–10% porosity. From composite theory, the effective thermal conductivity, k_{eff}, of such a two phase system assuming no thermal barrier resistance at the interface depends on the thermal conductivity of the matrix, k_{m}, the thermal conductivity of the particle, k_{p}, and the particle volume fraction, f_{p}, [8]

$$k_{\text{eff}} = k_{\text{m}} \frac{k_{\text{p}} + 2k_{\text{m}} + 2f_{\text{p}}(k_{\text{p}} - k_{\text{m}})}{k_{\text{p}} + 2k_{\text{m}} - f_{\text{p}}(k_{\text{p}} - k_{\text{m}})} \qquad (1)$$

The effective thermal conductivity was calculated for the three material systems under consideration here using Equation 1 and the respective thermal conductivity of each phase from Fig. 10. The result shows that k_{eff} is lowest for the ZrO_2 powder/SiC matrix, highest for Mo powder/SiC matrix, with the SiC powder/SiC matix intermediate between these (Fig. 11).

During SALDVI processing, temperatures in the laser heated process zone exceed 1000°C, and temperature gradients arise in the workpiece. The temperature gradients would be expected to be highest when

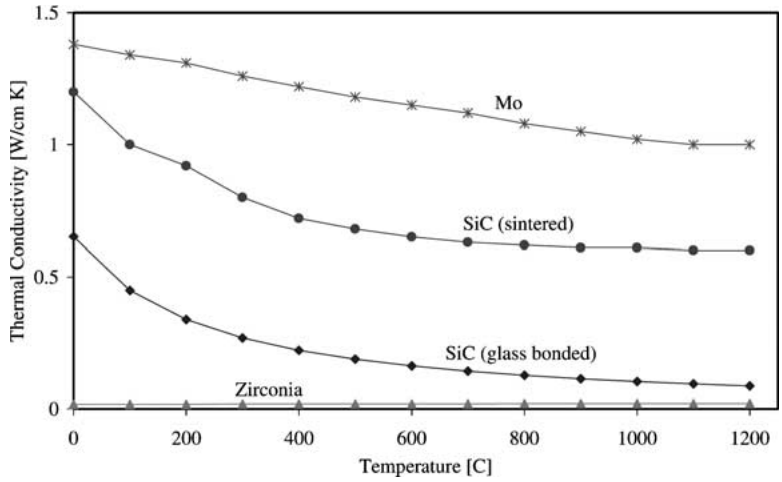

Figure 10 Thermal conductivity of SALDVI materials vs temperature [7].

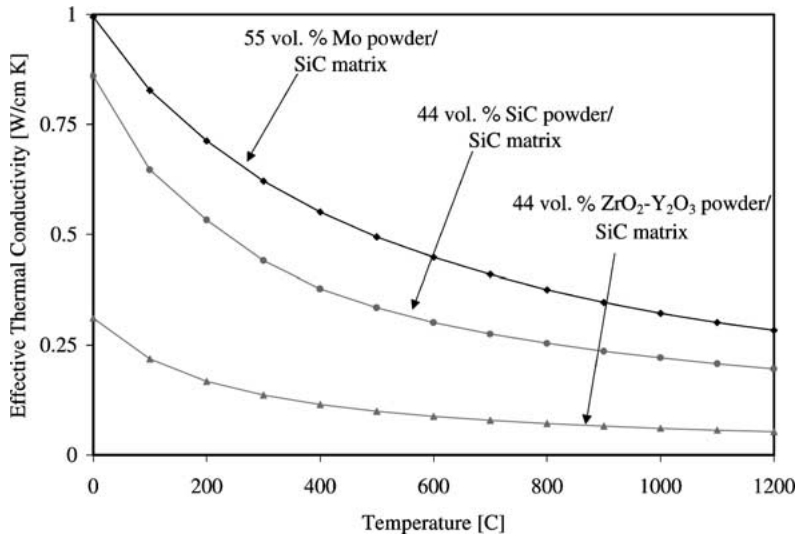

Figure 11 Effective thermal conductivity of SALDVI composites calculated using Equation 1.

k_{eff} is lowest, that is, the temperature gradients would be sharpest for the ZrO_2-Y_2O_3 powder sample, more gradual for the SiC powder sample, and broadest for the Mo powder sample. Upon cooling, which occurs continually as the laser scans across the workpiece and at the end of a pass when the laser turns off, the material contracts. However, contraction may be restrained by cooler material adjacent to the process zone, either within the same layer as in the slab geometry, or below due to previous layers as occurs with either bar or slab. Thus, different effective thermal conductivity in the three material systems could cause different magnitudes of thermal stress in the workpiece during SALDVI processing. The most severe cracking is observed in the ZrO_2-Y_2O_3 powder sample, which has the lowest effective thermal conductivity. Less severe cracking is observed in the SiC powder sample, and no cracks are seen for the Mo powder sample, which correlates well with the relative values of k_{eff} in Fig. 11.

A further point to consider regarding the relative susceptibility of the various material systems to thermal cracking involves the particle shape. The SiC and ZrO_2-Y_2O_3 powders are irregular in shape, while the Mo powder is spherical. A sharp corner of a particle would create a region of high stress concentration in the surrounding matrix. A spherical particle would create a blunt feature with a lower stress concentration. Thus, a crack would likely appear in the SiC or ZrO_2-Y_2O_3 powder sample at a lower thermal stress value than in the Mo powder sample. It was noted earlier that the surface appearance differs among the three materials. The surface topology of the SiC and ZrO_2-Y_2O_3 powder samples is rougher than that of the Mo powder sample, in both the bar and slab geometry. These features may also act as stress concentrations, lowering the stress needed to initiate a surface crack in the rougher samples. The cause of the rougher surface topology obtained when using the SiC and ZrO_2-Y_2O_3 powders is not clear. The Mo powder flows better than the SiC and ZrO_2-Y_2O_3powders because of its spherical shape, producing a smoother surface before infiltration begins. Also, displacement of some powders due to gas convection has been observed during infiltration, possibly due to bouyancy effects when pressure gradients arise in the gas phases within the powder bed. There is a three-fold increase in gas pressure when the $Si(CH_3)_4$ precursor molecule decomposes into solid SiC and methane. For the same size particle, the Mo powder is 3 times heavier

than the SiC, and twice as heavy as the zirconia. So the Mo powder is also more stable than the other two powders when gas convection occurs.

5. Conclusions

Thermal stress plays a major role in cracking in bar and slab samples of SiC matrix/SiC powder and SiC matrix/ZrO_2-Y_2O_3 powder made by SALDVI. The effective thermal conductivity of the SALDVI workpiece correlates well with the severity of thermal cracking. The lower k_{eff} the more severe the cracking. SiC matrix/Mo powder samples have the highest k_{eff}, and show no cracking. The irregular shape of the SiC and ZrO_2-Y_2O_3 powders, as well as a higher surface roughness, could provide stress risers in the matrix during processing, increasing their susceptibility to thermal cracking compared to the spherical Mo powder.

Acknowledgement

The authors acknowledge the support for this research by the Office of Naval Research (grant #N00014-95-1-0978).

References

1. B. R. BIRMINGHAM and H. L. MARCUS, in Proceedings of the Solid Freeform Fabrication Symposium, The University of Texas at Austin, 1994, p. 348.
2. J. E. CROCKER, S. L. HARRISON, L. SUN, L. L. SHAW and H. L. MARCUS, *JOM* **50** (1998) 21.
3. J. E. CROCKER, L. SUN, H. ANSQUER, L. L. SHAW and H. L. MARCUS, in Proceedings of the Solid Freeform Fabrication Symposium, The University of Texas at Austin, 1999, p. 495.
4. J. E. CROCKER, L. L. SHAW and H. L. MARCUS, in Proceedings of the Solid Freeform Fabrication Symposium, The University of Texas at Austin, 2000, p. 168.
5. J. E. CROCKER, S. L. HARRISON, L. SUN, L. L. SHAW and H. L. MARCUS, in Proceedings of TMS Ultrafine Grained Materials Symposium, Nashville, TN, March 2000.
6. Y. S. TOULOUKIAN, R. K. KIRBY, R. E. TAYLOR and P. D. DESAI, in "Thermophysical Properties of Matter, Vol. 12: Thermal Expansion Metallic Elements and Alloys" (IFI/Plenum, New York, 1975).
7. Y. S. TOULOUKIAN, R. W. POWELL, C. Y. HO and P. G. CLEMENS, in "Thermophysical Properties of Matter, Vol. 2: Thermal Conductivity Nonmetallic Solids" (IFI/Plenum, New York, 1970).
8. D. P. H. HASSELMAN and K. Y. DONALDSON, *J. Amer. Ceram. Soc.* **75**(11) (1992) 3137.

Received 3 June
and accepted 10 December 2001